Linear Covariance Analysis of Closed-loop Attitude Determination and Control System of Sub-Arcsec Pointing Three-Axes Spacecraft

Conference Paper · August 2019

CITATIONS
0

READS
321

1 author:

Divya Bhatia
The American Institute of Aeronautics and Astronautics
28 PUBLICATIONS **102** CITATIONS

SEE PROFILE

AAS 19-739

LINEAR COVARIANCE ANALYSIS OF CLOSED-LOOP ATTITUDE DETERMINATION AND CONTROL SYSTEM OF SUB-ARCSEC POINTING THREE-AXES SPACECRAFT

Divya Bhatia*

Error analysis is indispensable, specifically for missions requiring stringent system performances. In this paper linear covariance techniques are employed for the error analysis of the closed-loop Attitude Determination and Control System (ADCS) of a three-axes spacecraft of a DLR future mission named 'InfraRed Astronomy Satellite Swarm Interferometer' with a sub-arcsec pointing requirement. Components of its closed-loop ADCS includes a Multiplicative Kalman Filter which fuses the measurements from a three-axes rate-integrating gyroscope and a star tracker; a sliding mode controller that provides robust control in the presence of external disturbances like the gravity-gradient torque, the solar radiation pressure torque and a random disturbance torque; and reaction wheels for the spacecraft actuation. Various sources of errors include the gyro errors and the misalignments, the control bias and the wheel misalignments, external disturbance torques, a suboptimal filter with model replacement and a sliding mode controller that utilizes a saturation function. A dimensionally large state vector of the true state vector and the navigation state vector is created owing to their coupled dynamics which results in a linear time-varying model of the entire closed-loop system. Associated closed loop covariance analysis equations are formulated to determine the variances of the true and the expected attitude estimation errors, variances of the true pointing errors of the closed-loop system and the variances of the required control effort. These results are verified by the nonlinear Monte Carlo simulations. The implementation substantiates the claim that the linear covariance analysis is a useful tool for fast analysis of a closed-loop ADCS.

INTRODUCTION

Error analysis can be crucial during mission design by providing specifications of various system requirements. It becomes indispensable in the case of stringent requirements imposed on the spacecraft systems like the micro-meter ranging accuracy, the sub-arcsec to milli-arcsec pointing accuracy[1,2] etc. It is also necessary to determine the level of ground-based processing required to meet these stringent requirements. This also allows the analyst to judge the importance of various sources of error and make informed recommendations to reduce the effect of the largest contributors.

Missions with pointing accuracies better than sub-arcsec are becoming norm for the future space missions, like the Lisa Pathfinder, James Webb Space Telescope etc. One such mission with a high accuracy pointing requirement is the DLR (German Aerospace Center, Bonn) future mission named "InfraRed Astronomy Satellite Swarm Interferometer (IRASSI)",[1–4] which is an aperture synthesis interferometer constituting a 3D swarm of 5 satellites orbiting Sun-Earth Lagrange point 2 in a halo orbit. The science objective of this mission is to image the circumstellar disks and the protoplanetary regions at high resolution because these are fertile grounds for stars and planets genesis. High

*GNC Research Associate, Institute of Flight Guidance (IFF), Technical University of Braunschweig, Germany, 38108.

resolution images of these regions impose demanding attitude accuracies on the Attitude Determination and Control system (ADCS) of these space telescopes.This demanding attitude accuracy requirement of 0.4 arcsec (with a goal of 0.2 arcsec) for each IRASSI telescope (Figure 1b), can be separated into two parts, i.e. pointing accuracies from the Attitude Estimation System (AES) and the Attitude Control System (ACS) known as the Measurement Error (ME) and the Control Error (CE) respectively (as shown in Figure 1a). The AES and the ACS are the components of IRASSI's high accuracy ADCS as shown in Figure 2, that were independently designed and developed in references 3–5, which independently achieved stringent attitude estimation and control (best-case) accuracies of 0.03 and 0.02 arcsec (Table 1) respectively. The two mission modes of IRASSI are: 1) Precise Pointing Mode/Science Observation Mode and 2) Coarse Pointing/Acquisition Mode. During the precise pointing mode, scientific observations of the celestial targets are performed which requires the above mentioned stringent pointing accuracy. When the spacecraft is not in this mode, it is in the coarse pointing mode. Further details of these modes and this mission are explained in the references 2, 3 and 4.

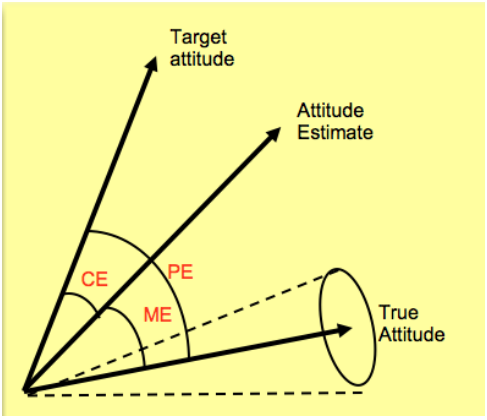

(a) Pointing definitions: Pointing Error (PE), Measurement Error (ME) and Control Error (CE).

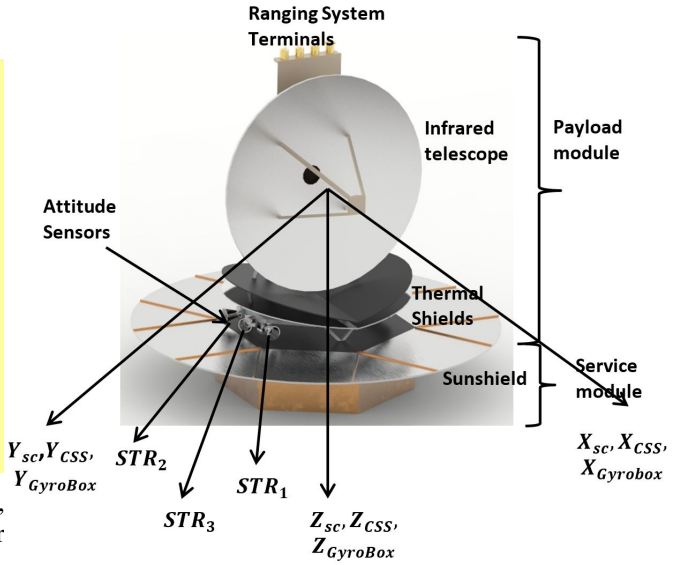

(b) IRASSI Spacecraft design with attitude sensors mounted onboard.

Figure 1: IRASSI Spacecraft Attitude System Specifications.

In this paper, an error analysis of the closed-loop ADCS of the IRASSI mission[2] for the precise pointing mode is performed. In this mode, once the pointing towards a celestial target is acquired, only small angle deviations denoted by error quaternion $\delta\mathbf{q}$[8] will occur due to various errors. Various sources of errors in its closed-loop ADCS are the errors from the gyro, the external disturbance torques from the gravity-gradient, the solar radiation pressure and a random disturbance moment to account for other unforeseeable or unmodeled disturbances,[2,5–7] the control bias and the reaction wheel misalignments, a suboptimal MEKF with model replacement and a Sliding Mode Controller (SMC) that provides suboptimal tracking performance due to the usage of a saturation function.[8] Linear covariance theory has been applied to the design and analysis of the orbit determination algorithms,[9] general estimation problems, inertial navigation systems, attitude determination systems and the closed-loop ADCS error analysis.[10] Linear covariance technique in the reference 10 was

produced by combining the developments in the linear covariance theory by Battin[11] with the continuous feedback control and the model replacement.[8] Reference 10 demonstrates the linear covariance techniques for a spin-stabilized spacecraft, which has been adapted for a three-axes spacecraft in this paper. The application of the linear covariance analysis to a three-axes spacecraft is demonstrated for a sub-arcsec pointing spacecraft of IRASSI mission, for which the sensors, actuators, filter algorithms, control algorithm, and its disturbances differ from the reference 10.

The novelty of this paper is manifold.

1. The quaternion multiplicative error is utilized as a state instead of the additive euler angle error because quaternion avoids any singularities for rotations between $0^\circ - 360^\circ$ as opposed to the euler angle,[8]
2. The quaternion-out star tracker measurement model is used even though the star tracker misalignments are not considered,
3. SMC is used as the controller in the linear covariance analysis which is robust towards the external disturbances but is more complex as compared to the usual proportional-derivative controller used in 10 because it involves additional terms involving saturation function which results in constant term in the linear covariance model(Eq. (60)) and the covariance propagation(Eq. (66)). This generalizes the linear covariance techniques for ADCS systems involving complex controllers which involve additional state-independent terms unlike in 10,
4. This analysis contains inertia uncertainty term which also contributes to the additional constant term in Eqs. (60) and (66),
5. This analysis is performed on a sub-arcsec pointing IRASSI mission, and
6. This analysis is generalized for a 3-axes spacecraft control which results in a linear-time varying model as compared to linear-time invariant model applied to a spin-stabilized spacecraft in 10. Consequently, the analysis performed in this work can be applied to any future missions requiring 3-axes spacecraft attitude control which is the case in most missions.

To develop the linear covariance simulation for IRASSI spacecraft, the truth models of the system dynamics, sensors and actuators are first defined in the next section. Biases, misalignments , scale-factors, and other colored noise processes are incorporated into these truth models. Next, the navigation state vector is defined, its associated navigation algorithm i.e. the Multiplicative Extended Kalman Filter with model replacement is developed, and a SMC is developed. All models and algorithms are linearized about their mean or nominal state time-history. Further a large dimension state vector is created by appending the navigation state vector to the true state vector owing to their coupled dynamics which results in a linear time-varying model of the entire closed-loop system. Associated closed loop covariance analysis equations are formulated including the covariance of the closed-loop control/pointing errors and the covariance of the control effort. The simulation results of this linear covariance analysis and the non-linear Monte Carlo analysis of its closed-loop ADCS are compared in the simulation section which is followed by the conclusion section.

IRASSI ATTITUDE MODEL

IRASSI's AES fuses the measurements from a high accuracy star tracker and a 3-axes rate-integrating gyroscope via a Multiplicative Extended Kalman Filter (MEKF),[3,4] where the quaternion is used as the attitude parameter due to its singularity free property for both estimation and the

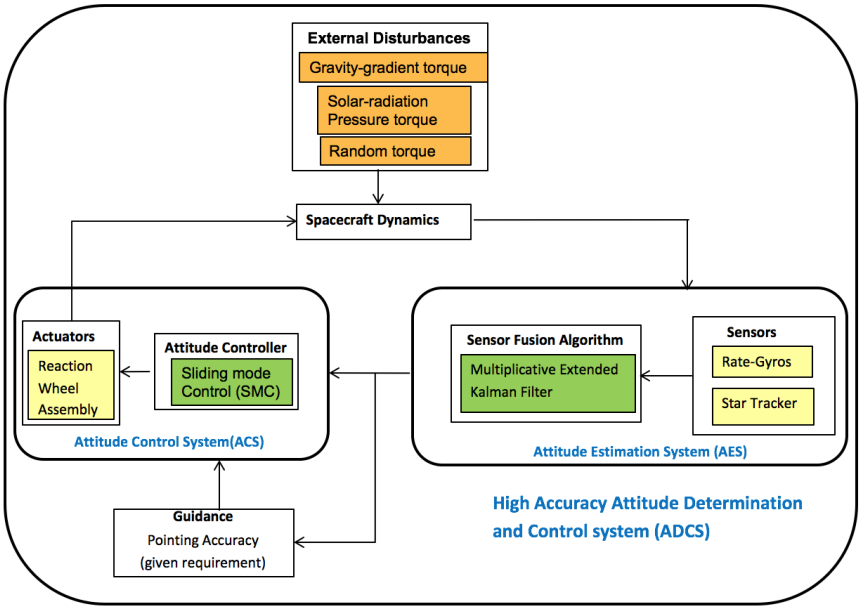

Figure 2: IRASSI's Attitude Determination and Control System (ADCS) Components.

Table 1: IRASSI spacecraft pointing accuracies achieved by individual attitude estimation and control systems.[2–4]

Spacecraft System	Accuracy achieved (arcsec)	Total accuracy required (arcsec)
Attitude Estimation	0.03 (best-case), 0.1 (worst-case)	0.4 (with a goal of 0.2)
Attitude Control	0.02 (best-case)	

control. Its ACS is composed of a first-order SMC,[5,8] that provides robustness towards the external disturbances like the gravity-gradient torque,[2,6] the solar radiation pressure torque[2,7] and a random torque which accounts for other unmodeled or unforeseen disturbances. Three reaction wheels in pyramid configuration provide actuation to the spacecraft for precise pointing, where a basic pseudoinverse distribution law[8] can be utilized to allocate the control torques provided by the SMC from the spacecraft 3-axes to the reaction wheels.

Linearized Attitude Dynamics Model

Assuming a rigid body motion, IRASSI's nonlinear rotational dynamics is given by

$$\mathbf{J}\dot{\boldsymbol{\omega}}^B = -[\boldsymbol{\omega}^B\times]\mathbf{J}\boldsymbol{\omega}^B + \boldsymbol{\tau}_w^B + \boldsymbol{\tau}_{SRP}^B + \boldsymbol{\tau}_{gg}^B + \boldsymbol{\tau}_{dist}^B \tag{1}$$

where the superscript B in the above equation denotes that the variable is expressed in the spacecraft body-fixed frame. We assume that all variables are expressed in the spacecraft body-fixed frame and drop it in the consequent paper for ease, unless otherwise stated. With the inertia uncertainty $\delta\mathbf{J}$ in the principal inertia tensor $\mathbf{J}_0$, the total inertia tensor in the x-y-z body frame is $\mathbf{J} = \mathbf{J}_0 + \delta\mathbf{J}$, where

$$\mathbf{J}_0 = \begin{bmatrix} 2059.5 & 0 & 0 \\ 0 & 5954.2 & 0 \\ 0 & 0 & 5974.3 \end{bmatrix} [kg.m^2], \quad \delta\mathbf{J} = -\begin{bmatrix} 250 & 0 & 0 \\ 0 & 250 & 0 \\ 0 & 0 & 250 \end{bmatrix} [kg.m^2] \tag{2}$$

$\boldsymbol{\tau}_{gg}$ is the gravity-gradient torque and $\boldsymbol{\tau}_{SRP}$ is the torque due to the solar radiation pressure.[2] Since the total value of $\boldsymbol{\tau}_{gg}$ and $\boldsymbol{\tau}_{SRP}$ is small and bounded($\leq 10^{-5}$ as shown in 2), they are neglected in this analysis. For missions where these torques are significant, they can also be linearized and incorporated in the state-space model(Eq. (26)). Hence, the nonlinear dynamics equation becomes

$$\mathbf{J}\dot{\boldsymbol{\omega}}^B = -[\boldsymbol{\omega}^B\times]\mathbf{J}\boldsymbol{\omega}^B + \boldsymbol{\tau}_w^B + \boldsymbol{\tau}_{dist}^B \tag{3}$$

$\boldsymbol{\tau}_{dist}$ is a zero mean continuous Gaussian white noise random disturbance moment that accounts for the unmodeled or unforeseen internal perturbations/vibrations and/or external disturbances.

$$\boldsymbol{\tau}_{dist} = \boldsymbol{\zeta}_d, \quad E\left[\boldsymbol{\zeta}_d(t)\boldsymbol{\zeta}_d^T(t')\right] = \mathbf{S}_d \cdot \delta(t-t') \tag{4}$$

$\boldsymbol{\tau}_w^B$ is the spacecraft 3-axes torque in the spacecraft body-fixed frame provided byreaction wheels, such that

$$\boldsymbol{\tau}_w^B = \boldsymbol{\tau}_N^B + \delta\boldsymbol{\tau}_w^B \tag{5}$$

where the perturbing torque is given as

$$\delta\boldsymbol{\tau}_w^B = (I_3 - [\boldsymbol{\epsilon}\times])\delta\boldsymbol{\tau}_{SMC}^B + \mathbf{b}_{act}^B + \boldsymbol{\zeta}_{act}^B \tag{6}$$

where $\delta\boldsymbol{\tau}_w^B$ and $\delta\boldsymbol{\tau}_{SMC}^B$ are the wheel control torques and the perturbed linearized SMC torques provided to the 3-axes spacecraft. $\mathbf{b}_{act}^B$ and $\boldsymbol{\epsilon}_{act}^B$ are the control bias and the reaction wheel misalignment matrix, initially random and constant thereafter, i.e. $\dot{\mathbf{b}}_{act}^B = \dot{\boldsymbol{\epsilon}}_{act}^B = 0$.

$\boldsymbol{\zeta}_{act}^B$ is the zero mean continuous Gaussian white noise with the variance

$$E\left[\boldsymbol{\zeta}_{act}(t)\boldsymbol{\zeta}_{act}^T(t')\right] = \mathbf{S}_{act} \cdot \delta(t-t') \tag{7}$$

With $\boldsymbol{\omega}_N = [\,\omega_{N1} \quad \omega_{N2} \quad \omega_{N3}\,]^T = [\,0 \quad 0 \quad 0\,]^T$ as the nominal angular velocity of the IRASSI spacecraft in the precise pointing mode (because in this mode, once the spacecraft is pointed at the target, it deviates from its attitude only little due to the external and internal disturbance torques), its nominal attitude dynamics becomes

$$\dot{\boldsymbol{\omega}}_{\boldsymbol{N}} = 0 = \mathbf{J}_0^{-1}\left(\boldsymbol{\tau}_N - [\boldsymbol{\omega}_N\times]\mathbf{J}_0\boldsymbol{\omega}_N\right) \tag{8}$$

Therefore the nominal control torque is $\boldsymbol{\tau}_N = [\boldsymbol{\omega}_N\times]\mathbf{J}_0\boldsymbol{\omega}_N$. The angular velocity perturbation is given by Eq. (9). Differentiating Eq. (9) and substituting Eqs. (6), (5) and (3) in it gives the remaining perturbation dynamics given by Eq. (10).

$$\delta\boldsymbol{\omega} \equiv \boldsymbol{\omega} - \boldsymbol{\omega}_N \tag{9}$$

$$\dot{\boldsymbol{\delta\omega}} = \mathbf{J}_0^{-1}\left(-[\boldsymbol{\omega}\times]\mathbf{J}_0\boldsymbol{\omega} + (I_3 - [\boldsymbol{\epsilon}\times])\delta\boldsymbol{\tau}_{SMC} + \mathbf{b}_{act} + \boldsymbol{\zeta}_{act} + \boldsymbol{\tau}_N + \boldsymbol{\zeta}_d\right) - \mathbf{J}_0^{-1}([\boldsymbol{\omega}\times]\delta\mathbf{J}\boldsymbol{\omega} + \delta\mathbf{J}\dot{\boldsymbol{\omega}}) \tag{10}$$

The linearized attitude dynamics are obtained by substituting Eq. (9) in Eq. (10) and neglecting the second and higher order terms as follows.

$$\dot{\boldsymbol{\delta\omega}} = \mathbf{J}_0^{-1}\left([\mathbf{J}_0\boldsymbol{\omega}_N\times] - [\boldsymbol{\omega}_N\times]\,\mathbf{J}_0\right)\delta\boldsymbol{\omega} + \mathbf{J}_0^{-1}(\delta\boldsymbol{\tau}_{SMC} + \mathbf{b}_{act} + \boldsymbol{\zeta}_{act} + \boldsymbol{\zeta}_d) - \mathbf{J}_0^{-1}[\boldsymbol{\omega}_N\times]\delta\mathbf{J}\boldsymbol{\omega}_N \tag{11}$$

Spacecraft nonlinear rotational motion kinematics and its linearized attitude kinematics with quaternions as the parameter are given by Eqs. (12) and (13) respectively.[8]

$$\dot{\mathbf{q}}_{1:3} = \frac{1}{2}(q_4\mathbf{I}_3 + [\mathbf{q}_{1:3}\times])\boldsymbol{\omega} \tag{12a}$$

$$\dot{q}_4 = -\frac{1}{2}\mathbf{q}_{1:3}^T\boldsymbol{\omega} \tag{12b}$$

$$\dot{\delta\boldsymbol{\upsilon}} = -\left[\boldsymbol{\omega}_N\times\right]\delta\boldsymbol{\upsilon} + \delta\boldsymbol{\omega} \tag{13}$$

where $\mathbf{q}^T\mathbf{q} = 1$ is the unit norm constraint of the unit quaternion and, $\delta\boldsymbol{\upsilon} = 2\delta\mathbf{q}_{1:3} = 2(\mathbf{q}\otimes\mathbf{q}_N^{-1})_{1:3}$ is the small angle rotation from the nominal vehicle attitude to the true vehicle attitude and is twice the vector part of the multiplicative quaternion error $\delta\mathbf{q}$.

Linearized Sliding Mode Control

SMC[8] is a controller that steers the system trajectory to a properly chosen sliding manifold and thereafter maintains the motion on the manifold by means of a control, thus exploiting the main features of the sliding mode, i.e. its insensitivity to external and internal disturbances matched by the control, ultimate accuracy, robustness to model uncertainties and finite-time convergence of the sliding variables to zero. For classical SMC, the chosen sliding surface is given as follows

$$\boldsymbol{\sigma} = \delta\boldsymbol{\omega} + \Lambda\,\mathrm{sign}(\delta q_4)\delta\mathbf{q}_{1:3} \tag{14}$$

where Λ is the sliding surface slope, $\delta\boldsymbol{\omega}$ is the angular velocity error, $\delta\mathbf{q}_{1:3}$ is the error vector quaternion, δq_4 is the scalar error quaternion component and $\mathrm{sign}(\delta q_4)$ is used to eliminate the *unwinding phenomenon*.[2,8] Taking the first time-derivative of $\boldsymbol{\sigma}$ introduces the linearized control $\delta\boldsymbol{\tau}_{SMC}$ in $\dot{\boldsymbol{\sigma}}$, giving

$$\dot{\boldsymbol{\sigma}} = \dot{\delta\boldsymbol{\omega}} + \Lambda\,\mathrm{sign}(\delta q_4)\dot{\delta\mathbf{q}}_{1:3} \tag{15}$$

where linearized $\dot{\delta\mathbf{q}}_{1:3}$ from reference 8 is given as follows.

$$\dot{\delta\mathbf{q}}_{1:3} = \frac{1}{2}\delta\boldsymbol{\omega} - \frac{1}{2}[\boldsymbol{\omega}_N\times]\delta\boldsymbol{\upsilon} \tag{16}$$

Substituting Eq. (11) in Eq. (15) gives

$$\dot{\boldsymbol{\sigma}} = \mathbf{J}_0^{-1}\left([(\mathbf{J}_0\boldsymbol{\omega}_N)\times] - [\boldsymbol{\omega}_N\times]\,\mathbf{J}_0\right)\delta\boldsymbol{\omega} + \mathbf{J}_0^{-1}(\delta\boldsymbol{\tau}_{SMC} + \mathbf{b}_{act} + \boldsymbol{\zeta}_{act} + \boldsymbol{\zeta}_d) - \mathbf{J}_0^{-1}[\boldsymbol{\omega}_N\times]\delta\mathbf{J}\boldsymbol{\omega}_N + \Lambda\,\mathrm{sign}(\delta q_4)\dot{\delta\mathbf{q}}_{1:3} \tag{17}$$

With the sliding mode dynamics $\dot{\boldsymbol{\sigma}} = 0$, the perturbing SMC torque is given as Eq. (18).

$$\delta\boldsymbol{\tau}_{SMC} = \left([\boldsymbol{\omega}_N\times]\,\mathbf{J}_0 - [(\mathbf{J}_0\boldsymbol{\omega}_N)\times] - \frac{\mathbf{J}_0\Lambda}{2}\,\mathrm{sign}(\delta q_4)\right)\delta\boldsymbol{\omega} + \frac{\mathbf{J}_0\Lambda}{2}\,\mathrm{sign}(\delta q_4)[\boldsymbol{\omega}_N\times]\delta\boldsymbol{\upsilon} - \mathbf{b}_{act} - \mathbf{J}_0\boldsymbol{\varepsilon}sat(\boldsymbol{\sigma}_i, e_{bl_i}) \tag{18}$$

where a discontinuous term $-\mathbf{J}_0\boldsymbol{\varepsilon}sat(\boldsymbol{\sigma}_i e_{bl_i})$ is added to account for the model uncertainties. That means the terms containing the moment of inertia uncertainty (i.e. $\delta\mathbf{J}$), the actuator noise (i.e. $\boldsymbol{\zeta}_{act}$) and the external disturbances (i.e. $\boldsymbol{\zeta}_d$) are removed from the $\delta\boldsymbol{\tau}_{SMC}$ as it is accounted by the discontinuous term. $sat(\boldsymbol{\sigma}_i, e_{bl_i})$ for $i = 1, 2, 3$ is the saturated function used to reduce the chattering phenomenon[2] with arguments as the sliding surface $\boldsymbol{\sigma}$ and e_{bl}. e_{bl} is the sliding surface

boundary layer and ε is a positive quantity.[8] Check references 8 and 2 for more details about SMC derivation process.

$$sat(\sigma_i, e_{bl_i}) = \begin{cases} -1, & \text{if } \sigma_i < -e_{bl_i} \\ \dfrac{|\sigma_i|}{e_{bl_i}}, & \text{if } |\sigma_i| \leq e_{bl_i} \\ 1, & \text{if } \sigma_i > e_{bl_i} \end{cases}$$

Linearized Rate-Gyro Measurement Model

Nonlinear gyro measurement model is given by[8]

$$\tilde{\boldsymbol{\omega}} = (I_3 + \mathbf{S})\boldsymbol{\omega} + \mathbf{b}_\omega + \boldsymbol{\zeta}_\omega \tag{19a}$$

$$\dot{\mathbf{b}}_\omega = \boldsymbol{\zeta}_b \tag{19b}$$

$$\mathbf{S} = \begin{bmatrix} \mathrm{s}_1 & \mathrm{k}_{U1} & \mathrm{k}_{U2} \\ \mathrm{k}_{L1} & \mathrm{s}_2 & \mathrm{k}_{U2} \\ \mathrm{k}_{L2} & \mathrm{k}_{L3} & \mathrm{s}_3 \end{bmatrix} \tag{19c}$$

where $\mathbf{S}$ is the matrix of scale factor vector $\mathbf{s} = [\, s_1 \quad s_2 \quad s_3 \,]^T$, upper misalignment vector $\mathbf{k}_U = [\, k_{U1} \quad k_{U2} \quad k_{U3} \,]^T$ and lower misalignment vector $\mathbf{k}_L = [\, k_{L1} \quad k_{L2} \quad k_{L3} \,]^T$. $\boldsymbol{\zeta}_\omega$ is the zero mean continuous Gaussian white noise with the variance

$$E\left[\boldsymbol{\zeta}_\omega(t)\boldsymbol{\zeta}_\omega^T(t')\right] = \mathbf{S}_\omega \cdot \delta(t - t') \tag{20}$$

The gyro drift bias $\mathbf{b}_\omega$ is a random process driven by zero mean continuous Gaussian white noise as given in Eq. (19)b with variance

$$E\left[\boldsymbol{\zeta}_b(t)\boldsymbol{\zeta}_b^T(t')\right] = \mathbf{S}_b \cdot \delta(t - t') \tag{21}$$

All the misalignments and scale factors are initially random and zero thereafter, such that

$$\dot{\mathbf{s}} = \dot{\mathbf{k}}_U = \dot{\mathbf{k}}_L = 0 \tag{22}$$

With $\delta\tilde{\boldsymbol{\omega}} \equiv \tilde{\boldsymbol{\omega}} - \boldsymbol{\omega}_N$ as the measurement perturbation relative to the nominal state, the linearized gyro measurement equation becomes

$$\delta\tilde{\boldsymbol{\omega}} = \delta\boldsymbol{\omega} + \mathbf{b}_\omega + \boldsymbol{\zeta}_\omega + \mathbf{D}\mathbf{s} + \mathbf{A}_{kU}\mathbf{k}_U + \mathbf{A}_{kL}\mathbf{k}_L \tag{23}$$

where $\mathbf{D} \equiv diag(\boldsymbol{\omega}_N)$, $\mathbf{A}_{kU} \equiv \begin{bmatrix} \omega_{N2} & \omega_{N3} & 0 \\ 0 & 0 & \omega_{N3} \\ 0 & 0 & 0 \end{bmatrix}$ and $\mathbf{A}_{kL} \equiv \begin{bmatrix} 0 & 0 & 0 \\ \omega_{N1} & 0 & 0 \\ 0 & \omega_{N1} & \omega_{N2} \end{bmatrix}$.

Linearized Star Tracker Measurement Model

IRASSI is equipped with three star trackers, where one star tracker can operate independently or two star trackers can operate simultaneously.[4] Second and/or third star trackers are provided for redundancy.[3,4] For this paper, one star tracker STR_1 (Figure 1b) whose boresight is aligned with the IRASSI telescope boresight direction is considered. Additionally, quaternion-out star trackers are considered in this work which is the capability provided by many modern-day star trackers along with its associated error covariances. Hence the quaternion-out star tracker measurement is given as the sum of the small angle error and the measurement noise.

$$\mathbf{z} = \delta\mathbf{q}(\delta\boldsymbol{\upsilon}) + \mathbf{v} \tag{24}$$

where no star-tracker misalignments are considered.

Linearized State Space Representation

The state space of the true perturbations from the nominal state is

$$\delta\mathbf{x}_{(3\mathbf{N}_x\times 1)} \equiv \mathbf{x} - \mathbf{x}_N = [\delta\boldsymbol{\upsilon}^T \;\; \delta\boldsymbol{\omega}^T \;\; \mathbf{b}_{act}^T \;\; \boldsymbol{\epsilon}_{act}^T \;\; \mathbf{b}_{\omega}^T \;\; \mathbf{k}_U^T \;\; \mathbf{k}_L^T \;\; \mathbf{s}^T]^T \tag{25}$$

where $\mathbf{N}_x = 8$ is the number of true states and the first state is not additive but multiplicative error. The linearized dynamics are given by

$$\delta\dot{\mathbf{x}} = \mathbf{A}\cdot\delta\mathbf{x} + \mathbf{G}\cdot\delta\boldsymbol{\tau}_{SMC} + \mathbf{B}\cdot\boldsymbol{\zeta} + \mathbf{G}\cdot\Delta\boldsymbol{\omega} \tag{26}$$

where $\boldsymbol{\zeta}$ is the continuous white process noise

$$\boldsymbol{\zeta} = [\boldsymbol{\zeta}_{\omega}^T \;\; \boldsymbol{\zeta}_b^T \;\; \boldsymbol{\zeta}_{act}^T \;\; \boldsymbol{\zeta}_d^T]^T \tag{27}$$

with variance

$$E\left[\boldsymbol{\zeta}(t)\boldsymbol{\zeta}^T(t')\right] = \mathbf{S}\cdot\delta(t-t') \tag{28}$$

The linearized star-tracker measurement equation is

$$\delta\mathbf{z} = \mathbf{H}\cdot\delta\mathbf{x} + \mathbf{v} \tag{29}$$

where the measurement noise is given by

$$\mathbf{v} = [\nu_1 \;\; \nu_2 \;\; \nu_3]^T \tag{30}$$

with variance

$$E\left[\mathbf{v}(t_i)\mathbf{v}(t_j)\right] = \mathbf{R}\cdot\delta_{ij} \tag{31}$$

The linearized gyro measurement equation is

$$\delta\tilde{\boldsymbol{\omega}} = \mathbf{H}_{gyro}\cdot\delta\mathbf{x} + \boldsymbol{\zeta}_{\omega} \tag{32}$$

Finally, the linearized control is given as

$$\delta\boldsymbol{\tau}_{SMC} = \mathbf{G}_x\cdot\delta\mathbf{x} + \Delta\boldsymbol{\tau} \tag{33}$$

where the terms $\mathbf{A}, \mathbf{B}, \mathbf{H}$, $\mathbf{H}_{gyro}$, $\mathbf{G}$, $\mathbf{G}_x$, $\Delta\boldsymbol{\omega}$ and $\Delta\boldsymbol{\tau}$ are provided in the appendix.

IRASSI NAVIGATION AND CONTROL DESIGN

Reduced Order Filter Algorithm with the Model Replacement

The filter design model assumes that the true misalignments, scale factors and control biases are zero as follows.

$$\mathbf{b}_{act_f} = \epsilon_{act_f} = \mathbf{k}_{U_f} = \mathbf{k}_{L_f} = \mathbf{s}_f = 0 \tag{34}$$

Thus the dynamics of the linearized states are

$$\dot{\delta\boldsymbol{\upsilon}}_f = -\left[\boldsymbol{\omega}_N\times\right]\delta\boldsymbol{\upsilon}_f + \delta\boldsymbol{\omega}_f \tag{35}$$

$$\dot{\boldsymbol{\delta\omega}}_f = \mathbf{J}_0^{-1}\left(\left[\mathbf{J}_0\boldsymbol{\omega}_N\times\right] - \left[\boldsymbol{\omega}_N\times\right]\mathbf{J}_0\right)\delta\boldsymbol{\omega}_f + \mathbf{J}_0^{-1}\delta\boldsymbol{\tau}_{SMC} + \mathbf{J}_0^{-1}(\boldsymbol{\zeta}_{act_f} + \boldsymbol{\zeta}_{d_f}) - \mathbf{J}_0^{-1}[\boldsymbol{\omega}_N\times]\delta\mathbf{J}\boldsymbol{\omega}_N \tag{36}$$

$$\dot{\mathbf{b}}_{\omega_f} = \boldsymbol{\zeta}_{b_f} \tag{37}$$

where $\delta\boldsymbol{\upsilon}_f = 2\delta\mathbf{q}_{1:3_f} = 2(\mathbf{q}_f \otimes \mathbf{q}_N^{-1})_{1:3}$ and $\delta\boldsymbol{\omega}_f \equiv \boldsymbol{\omega}_f - \boldsymbol{\omega}_N$. The linearized gyro measurements are

$$\delta\tilde{\boldsymbol{\omega}}_f \cong \delta\boldsymbol{\omega}_f + \mathbf{b}_{\omega_f} + \boldsymbol{\zeta}_{\omega_f} \tag{38}$$

But when the uncertainties in the rotational dynamics model (Eq. (36)) are significant, like the spacecraft inertia uncertainties, external disturbances etc., which is the case for IRASSI, the rotational dynamics are replaced by the gyro data.[3,4,8] Then the dynamical model for the filter design involves Eqs. (35), (37) and (38). Additionally, using the gyro model as the dynamic replacement provides autonomy where this filter can be computed on-board as it requires much less computations. Hence the spacecraft angular velocity estimate is given as

$$\delta\hat{\boldsymbol{\omega}}_f = (\delta\tilde{\boldsymbol{\omega}}_f - \hat{\mathbf{b}}_{\omega_f}) \tag{39}$$

This angular velocity estimate is utilized in the SMC as explained in the next section.

Using this model replacement,[8] the state space and the state dynamics for the filter design becomes

$$\delta\mathbf{x}_f = [\delta\boldsymbol{\upsilon}_f^T \quad \mathbf{b}_{\omega_f}^T]^T \tag{40}$$

$$\delta\dot{\mathbf{x}}_f = \mathbf{A}_f \cdot \delta\mathbf{x}_f + \mathbf{G}_\omega \cdot \delta\tilde{\boldsymbol{\omega}}_f + \mathbf{B}_f \cdot \boldsymbol{\zeta}_f \tag{41}$$

where $\mathbf{A}_f, \mathbf{G}_\omega$ and $\mathbf{B}_f$ are provided in the appendix and $\boldsymbol{\zeta}_f$ is a zero mean continuous white noise

$$\boldsymbol{\zeta}_f = \begin{bmatrix} \boldsymbol{\zeta}_{\omega_f} \\ \boldsymbol{\zeta}_{b_f} \end{bmatrix}, \quad E\left[\boldsymbol{\zeta}_f(t)\boldsymbol{\zeta}_f^T(t')\right] = \mathbf{S}_f \cdot \delta(t - t') \tag{42}$$

The star tracker measurements remain unchanged for the filter design and are given as

$$\delta\mathbf{z}_f = \mathbf{H}_f \cdot \delta\mathbf{x}_f + \mathbf{v}_f \tag{43}$$

where $\mathbf{H}_f$ is given in the appendix, and $\mathbf{v}_f$ is a zero mean discrete white noise

$$\mathbf{v}_f = [\nu_1 \;\; \nu_2 \;\; \nu_3]^T, \quad E\left[\mathbf{v}_f(t_i)\mathbf{v}_f(t_j)\right] = \mathbf{R}_f \cdot \delta_{ij} \tag{44}$$

This new design model is utilized to develop a Kalman filter algorithm. The state propagation equations are given by

$$\dot{\delta\hat{\mathbf{x}}}_f = \mathbf{A}_f \cdot \delta\hat{\mathbf{x}}_f + \mathbf{G}_\omega \cdot \delta\tilde{\boldsymbol{\omega}}_f \tag{45}$$

where

$$\delta\hat{\mathbf{x}}_f = [\delta\hat{\boldsymbol{\upsilon}}_f^T \quad \hat{\mathbf{b}}_{\omega_f}^T]^T = [(\hat{\mathbf{q}}_f \otimes \mathbf{q}_N^{-1})_{1:3} \quad \hat{\mathbf{b}}_{\omega_f}^T]^T \tag{46}$$

Now the filter navigation error is the residual error given as

$$\hat{\boldsymbol{\varepsilon}}_f \equiv \delta\hat{\mathbf{x}}_f - \delta\mathbf{x}_f \tag{47}$$

$$\dot{\hat{\boldsymbol{\varepsilon}}}_f = \mathbf{A}_f \cdot \hat{\boldsymbol{\varepsilon}}_f - \mathbf{B}_f \cdot \boldsymbol{\zeta}_f \tag{48}$$

The navigation error is expected to have zero mean and covariance given by

$$\mathbf{P}_f = E\left[\hat{\boldsymbol{\varepsilon}}_f \cdot \hat{\boldsymbol{\varepsilon}}_f^T\right] \tag{49}$$

where the filter state error covariance propagation is given as

$$\dot{\mathbf{P}} = \mathbf{A}_f \mathbf{P}_f + \mathbf{P}_f \mathbf{A}_f^T + \mathbf{B}_f \mathbf{S}_f \mathbf{B}_f^T \tag{50}$$

Kalman filter update equations for the post measurement state and the covariance corrections are given by

$$\mathbf{K}_f = \mathbf{P}_f \mathbf{H}_f^T (\mathbf{H}_f \mathbf{P}_f \mathbf{H}_f^T + \mathbf{R}_f)^{-1} \tag{51}$$

$$\mathbf{P}_f^+ = (I - \mathbf{K}_f \mathbf{H}_f) \mathbf{P}_f (I - \mathbf{K}_f \mathbf{H}_f)^T + \mathbf{K}_f \mathbf{R}_f \mathbf{K}_f^T \tag{52}$$

$$\delta \hat{\mathbf{x}}_f^+ = \delta \hat{\mathbf{x}}_f + \mathbf{K}_f (\delta \mathbf{z} - \delta \hat{\mathbf{z}}_f) \tag{53}$$

where

$$\delta \hat{\mathbf{z}}_f = \mathbf{H}_f \cdot \delta \hat{\mathbf{x}}_f \tag{54}$$

Since multiplicative error vector quaternion $\delta \boldsymbol{\upsilon}$ is used as a state, the full quaternion is updated as follows.[8]

$$\delta \hat{\mathbf{q}}_{1:3_f} = \frac{\delta \hat{\boldsymbol{\upsilon}}_f}{2}, \quad \delta \hat{\mathbf{q}}_{1:4_f} = \left[\delta \hat{\mathbf{q}}_{1:3_f} \quad \sqrt{1 - \delta \hat{\mathbf{q}}_{1_f}^2 - \delta \hat{\mathbf{q}}_{2_f}^2 - \delta \hat{\mathbf{q}}_{3_f}^2} \right] \tag{55}$$

$$\hat{\mathbf{q}}_f^* = \delta \hat{\mathbf{q}}_{1:4_f} \otimes \mathbf{q}, \quad \hat{\mathbf{q}}_f^+ = \hat{\mathbf{q}}_f^* / ||\hat{\mathbf{q}}_f^*|| \tag{56}$$

And a reset of these updated states is performed to transfer the information to the full state quaternion and gyro drift state as shown in reference 8. Since the covariance propagation and gain calculation are based on the reduced model with model replacement, this filter is no longer optimal. The effects of these suboptimal schemes on the true navigation errors is determined by linear covariance analysis. This is measured by comparing the filter covariance $\mathbf{P}_f$ to the true covariance $\mathbf{P}_{true}$ of the true filter state error.

Linearized Modified Sliding Mode Controller

With the states estimates $\delta \hat{\boldsymbol{\upsilon}}_f$ and $\hat{\mathbf{b}}_{\omega_f}$ known from the navigation filter above, the linearized SMC is modified as follows.

$$\delta \boldsymbol{\tau}_{SMC} = \left([\boldsymbol{\omega}_N \times] \mathbf{J}_0 - [(\mathbf{J}_0 \boldsymbol{\omega}_N) \times] - \frac{\mathbf{J}_0 \Lambda}{2} \operatorname{sign}(\delta \hat{q}_{f_4}) \right) (\delta \tilde{\boldsymbol{\omega}} - \hat{\mathbf{b}}_{\omega_f}) + \frac{\mathbf{J}_0 \Lambda}{2} \operatorname{sign}(\delta \hat{q}_{f_4}) [\boldsymbol{\omega}_N \times] \delta \hat{\boldsymbol{\upsilon}}_f - \mathbf{J}_0 \boldsymbol{\varepsilon} sat(\hat{\boldsymbol{\sigma}}_i, e_{bl_i}) \tag{57}$$

The sliding surface is $\hat{\boldsymbol{\sigma}} = \delta \hat{\boldsymbol{\omega}}_f + \Lambda \operatorname{sign}(\delta \hat{q}_{f_4}) \delta \hat{\mathbf{q}}_{f_{1:3}}$ and $\delta \hat{\boldsymbol{\omega}}_f$ is used from Eq. (39), where $\delta \tilde{\boldsymbol{\omega}}_f$ is the actual gyro measurement model $\delta \tilde{\boldsymbol{\omega}}$ from Eq. (23). The $\mathbf{b}_{act}$ in Eq. (18) is removed in Eq. (57) because it is zero according to Eq. (34). This can be written in the state-space form as follows.

$$\delta \boldsymbol{\tau}_{SMC} = \mathbf{G}_{f_{\hat{x}}} \cdot \delta \hat{\mathbf{x}}_f + \mathbf{A}_{f_\tau} \delta \tilde{\boldsymbol{\omega}} + \Delta \boldsymbol{\tau}_f \tag{58}$$

$\mathbf{G}_{f_{\hat{x}}}$, $\mathbf{A}_{f_\tau}$ and $\Delta \boldsymbol{\tau}_f$ are given in the appendix.

LINEAR COVARIANCE ANALYSIS

IRASSI Linear Covariance Model

For the linear covariance analysis, a dimensionally large vector $\mathbf{X} \in \mathbb{R}^{\mathbf{n}+\hat{\mathbf{n}}}$ comprised of the true state vector $\delta\mathbf{x}$ (Eq. (25)) and the navigation state vector $\delta\hat{\mathbf{x}}_f$ (Eq. (46)) is created as follows

$$\mathbf{X} \equiv \begin{bmatrix} \delta\mathbf{x} \\ \delta\hat{\mathbf{x}}_f \end{bmatrix} \tag{59}$$

Thus the true states and the navigation states can be extracted from the large state $\mathbf{X}$ by using appropriate mappings $\mathbf{M}_x$ and $\mathbf{M}_f$ such that $\delta\mathbf{x} = \mathbf{M}_x\mathbf{X}$ and $\delta\hat{\mathbf{x}}_f = \mathbf{M}_f\mathbf{X}$. The dynamics of the state $\mathbf{X}$ is defined as

$$\dot{\mathbf{X}} = \mathcal{A}\mathbf{X} + \mathcal{B}\boldsymbol{\zeta} + \mathcal{C} \tag{60}$$

with

$$\boldsymbol{\zeta} = \begin{bmatrix} \boldsymbol{\zeta}_\omega^T & \boldsymbol{\zeta}_b^T & \boldsymbol{\zeta}_{act}^T & \boldsymbol{\zeta}_d^T \end{bmatrix}^T \tag{61}$$

and

$$\mathcal{A} = \begin{bmatrix} \mathbf{A} + \mathbf{G}\mathbf{G}_{\boldsymbol{\tau}gyro} & \mathbf{G}\mathbf{G}_{f_{\hat{x}}} \\ \mathbf{A}_{fX} & \mathbf{A}_f \end{bmatrix}, \quad \mathcal{B} = \begin{bmatrix} \mathbf{B} + \mathbf{G}\mathbf{B}_\tau \\ \mathbf{B}_{fX} \end{bmatrix}, \quad \mathcal{C} = \begin{bmatrix} \mathbf{G}\Delta\mathbf{X} \\ 0_{6\times 1} \end{bmatrix} \tag{62}$$

where $\mathbf{G}_{\boldsymbol{\tau}gyro}$, $\mathbf{B}_\tau$ $\mathbf{B}_{fX}$, $\Delta\mathbf{X}$ and $\mathbf{A}_{fX}$ are provided in the appendix. And since

$$E[\delta\mathbf{x}] = E[\mathbf{x} - \mathbf{x}_N] = 0 \tag{63}$$

$$E[\delta\hat{\mathbf{x}}_f] = E[\hat{\mathbf{x}}_f - \mathbf{M}\mathbf{x}_N] = 0 \tag{64}$$

then the mean of the large state vector $E[\mathbf{X}] = 0$ and the covariance of the system can be calculated as

$$\mathbf{C}_A = E[\mathbf{X}(t)\mathbf{X}^T(t)] \tag{65}$$

The entire closed-loop system is represented by a linear time-varying differential equation (60) and a variety of linear system analysis can now be applied to this system. For the covariance analysis, the propagation and the update equations are as follows.

$$\dot{\mathbf{C}}_A = \mathcal{A}\mathbf{C}_A + \mathbf{C}_A\mathcal{A}^T + \mathcal{B}\mathbf{S}\mathcal{B}^T + \mathcal{C}\mathcal{C}^T \tag{66}$$

$$\mathbf{C}_A^+ = (I + \mathcal{K}\mathcal{H})\mathbf{C}_A(I + \mathcal{K}\mathcal{H})^T + \mathcal{K}\mathbf{R}_f\mathcal{K}^T \tag{67}$$

$$\mathcal{K} = \begin{bmatrix} 0 \\ \mathbf{K}_f \end{bmatrix}, \quad \mathcal{H} = [\mathbf{H} \quad -\mathbf{H}_f] \tag{68}$$

The initial conditions are defined as

$$\mathbf{C}_{A_0} = \begin{bmatrix} \mathbf{P}_{disp_0} & 0_{N_x\times N_f} \\ 0_{N_f\times N_x} & 0_{N_f\times N_f} \end{bmatrix}, \quad \mathbf{P}_{disp_0} = E[\delta\mathbf{x}_0\delta\mathbf{x}_0^T] \tag{69}$$

where the filter states are initiated with the state nominal values and zero variance.

Performance Evaluation

This section is same as in reference 10, but is mentioned here for clarity and completeness. The overall performance of the closed-loop ADCS is evaluated by examining the covariance matrix of the state $\mathbf{X}$ using appropriate mappings. The covariance of the true state dispersions $\delta\mathbf{x} = \mathbf{M}_x\mathbf{X}$ are given as

$$\mathbf{D}_{true} = E\left[\delta\mathbf{x}(t)\delta\mathbf{x}^T(t)\right] = \mathbf{M}_x\mathbf{C}_A\mathbf{M}_x^T \tag{70}$$

which accounts for the navigation errors, the guidance/control execution errors, and all the external disturbances/noise sources. Similarly, the covariance matrix of the navigation state dispersion $\delta\hat{\mathbf{x}}_f = \mathbf{M}_f\mathbf{X}$ is given as

$$\mathbf{D}_{nav} = E\left[\delta\hat{\mathbf{x}}_f(t)\delta\hat{\mathbf{x}}_f^T(t)\right] = \mathbf{M}_f\mathbf{C}_A\mathbf{M}_f^T \tag{71}$$

Filter estimation error which is the difference between the navigation state vector and the corresponding true state vector is given as

$$\mathbf{e}_{true} \equiv \delta\hat{\mathbf{x}}_f - \mathbf{M}\delta\mathbf{x} = \mathbf{M}_{true}\mathbf{X} \tag{72}$$

and its covariance matrix is given by

$$\mathbf{P}_{true} = E[\mathbf{e}_{true}\mathbf{e}_{true}^T]^T = \mathbf{M}_{true}\mathbf{C}_A\mathbf{M}_{true}^T \tag{73}$$

where $\mathbf{M}_{true} = \mathbf{M}_f - \mathbf{M}\mathbf{M}_x$. The control effort obtained as $\delta\boldsymbol{\tau}_{SMC} = \mathbf{M}_\tau \cdot \mathbf{X} + \mathbf{B}_\tau \cdot \boldsymbol{\zeta} + \Delta\boldsymbol{\tau}_f$.The covariance matrix of the control effort is given as

$$\mathbf{P}_\tau = E[\delta\boldsymbol{\tau}_{SMC}\delta\boldsymbol{\tau}_{SMC}^T] = \mathbf{M}_\tau\mathbf{C}_A\mathbf{M}_\tau^T + \mathbf{B}_\tau\mathbf{S}\mathbf{B}_\tau^T \tag{74}$$

where $\mathbf{M}_\tau = \mathbf{G}_{\boldsymbol{\tau}gyro} \cdot \mathbf{M}_x + \mathbf{G}_{f\hat{x}} \cdot \mathbf{M}_f$.

SIMULATION RESULTS

Setup

The simulations are performed for 2 hours of precise pointing mode of IRASSI spacecraft which is small angle regulation, hence the desired value of the angular velocity in all 3-axes are zero. Other non-zero desired values are for attitude angle. The nominal values of all the initial true states are zero except non-zero attitude angle states. All initial non-zero nominal values, initial uncertainties, process noise power-spectral-densities and other system parameters are given in Table 2. The initial filter states is $\mathbf{x}_f(0) = \mathbf{M}\mathbf{x}_0$. The initial true state covariance $\mathbf{P}_{disp_0}$ is a 24×24 diagonal matrix given in the appendix and the initial navigation filter covariance is $\mathbf{P}_{f_0} = \mathbf{M}\mathbf{P}_{disp_0}\mathbf{M}^T$. Now the power-spectral-densities of the true model process noise, the filter model process noise and the variance of the measurement noise respectively are given as follows.

$$\mathbf{S}_\eta = blkdiag(\mathbf{Q}_\omega \quad \mathbf{Q}_b \quad \mathbf{Q}_{act} \quad \mathbf{Q}_d) \tag{75}$$

$$\mathbf{S}_f = blkdiag(\mathbf{Q}_\omega \quad \mathbf{Q}_b) \tag{76}$$

$$\mathbf{R} = \mathbf{R}_f = \boldsymbol{\sigma}_{st}^2 I_3 \tag{77}$$

Table 2: Simulation Setup values.

Symbol	Value (for all 3-axes)	Units	Description
$\boldsymbol{\omega}_0$	0	$radian/sec$	Initial nominal angular velocities
$\boldsymbol{\theta}_0$	12	$degree$	Initial nominal attitude angles
$\boldsymbol{\omega}_d$	0	$radian/sec$	Desired angular velocities
$\boldsymbol{\theta}_d$	11	$degree$	Desired attitude angles
$\boldsymbol{\sigma}_{\delta\boldsymbol{\upsilon}}$	$\mathbf{q}_0 \otimes \mathbf{q}_d^{-1}$	$arcsec$	Initial attitude error 1-σ
$\boldsymbol{\sigma}_{\delta\boldsymbol{\omega}}$	0	deg/sec	Initial angular velocity 1-σ
$\boldsymbol{\sigma}_{b_{act}}$	0.0001	$N \cdot m$	Initial actuator bias 1-σ
$\boldsymbol{\sigma}_{\boldsymbol{\epsilon}_{act}}$	1	$arcsec$	Initial actuator misalignment 1-σ
$\boldsymbol{\sigma}_{b_{\boldsymbol{\omega}}}$	1	$arcsec/sec$	Initial gyro bias 1-σ
$\boldsymbol{\sigma}_{k_U}$	2000	$ppm(parts\ per\ million)$	Initial gyro upper-misalignment 1-σ
$\boldsymbol{\sigma}_{k_L}$	1000	ppm	Initial gyro lower-misalignment 1-σ
$\boldsymbol{\sigma}_s$	1000	ppm	Initial gyro scale factor 1-σ
$\boldsymbol{\sigma}_{ST}$	0.2	$arcsec$	Measurement noise 1-σ
$\mathbf{Q}_{\boldsymbol{\omega}}$	0.0005^2	$(deg/min)^2$	Gyro drift noise strength
$\mathbf{Q}_b$	0.0001^2	$(deg/hr)^2$	Gyro bias noise strength
$\mathbf{Q}_{act}$	0.01^2	$(N \cdot m)^2 \cdot sec$	Actuator noise strength
$\mathbf{Q}_d$	0.01^2	$(N \cdot m)^2 \cdot sec$	Disturbance noise strength
$\boldsymbol{\epsilon}$	10^{-4}		Positive quantity used in SMC
$\boldsymbol{\Lambda}$	0.9		Sliding surface slope used in SMC
e_{bl}	10^{-4}	$arcsec$	Sliding surface boundary layer used in SMC

Linear Covariance Results

Attitude Navigation Errors Attitude navigation errors from the linear covariance analysis are depicted in Figure 3a. The x-axis, y-and z-axes steady-state navigation $1-\sigma$ errors are 0.06 arcsec, 0.02 arcsec and 0.02 arcsec respectively. Whereas the filter $1-\sigma$ error is 0.01 arcsec in all 3-axes of the IRASSI spacecraft. It is clear that suboptimal, reduced order filter is underestimating the navigation error.

Attitude Dispersion Although attitude navigation errors are important, the final goal is to limit the attitude control system pointing errors,i.e., the attitude dispersion from their desired nominal values. Figure 3b compares the $1-\sigma$ true attitude dispersions to the $1-\sigma$ filter attitude dispersions. It demonstrates that the true attitude dispersions in the x-, y-, and z-axes are 0.06 arcsec, 0.02 arcsec and 0.02 arcsec respectively. This should be compared to the 0.4 arcsec pointing accuracy requirement for fine-pointing mode. The navigation and the true attitude errors are same, but are much below the required pointing accuracy of 0.4 arcsec.

Gyro Bias Errors Figure 4a depicts that the $1-\sigma$ filter gyro bias estimation errors in 3-axes spacecraft is 0, which is less than the filter $1-\sigma$ bias estimation error of 0.000003 arcsec/sec.

Control Effort and Reaction wheel demand Figure 4b shows the $1-\sigma$ control effort. After an initial transient, the steady-state variance in all 3-axes is approximately 0.0012 Nm. The steady-state control is primarily in response to actuator errors and random disturbances.

Nonlinear Monte Carlo Analysis

For IRASSI, the Monte Carlo (MC) simulation consists of the nonlinear dynamics and kinematics Eqs. (3) and (12) respectively, nonlinear gyro and quaternion-out star-tracker measurements

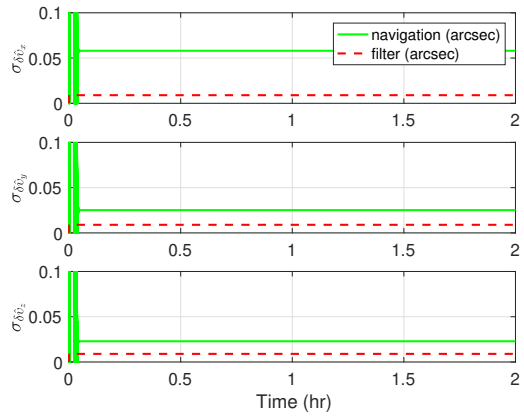

(a) Navigation Attitude dispersion.

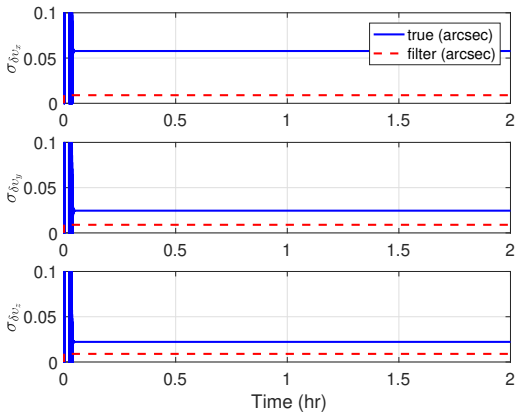

(b) True attitude dispersion.

Figure 3: Dispersion for attitude of 3-axes spacecraft. The red curve shows filter 1-σ error, blue curve shows the true 1-σ error and green curve shows the navigation 1-σ error.

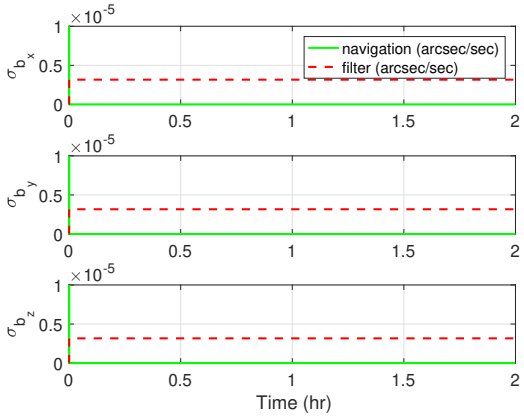

(a) Gyro drift estimation error. The red curve shows filter 1-σ error and green curve shows the navigation 1-σ error.

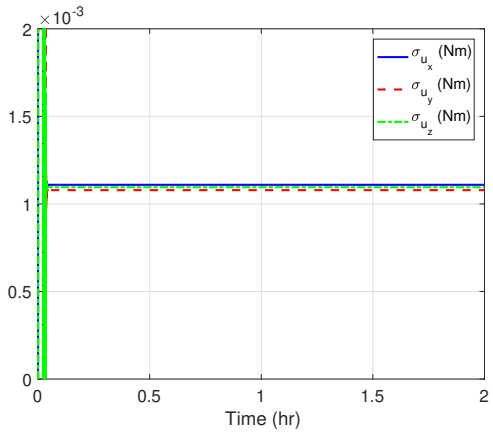

(b) 3-axes 1-σ control effort.

Figure 4: Linear Covariance Analysis for 3-axes spacecraft.

given by Eqs. (19) and (24) respectively, an Extended Kalman filter with reduced filter state and model replacement and an SMC control law based on the estimated attitude quaternion and the estimated angular rate with gyro bias compensation. For nonlinear MC analysis of linear covariance technique,[10] the covariance of the true dispersion and error states are computed by generating N samples of each state as a function of time and the covariances are given by Eqs. 80-82 in reference 10. $N = 1000$ MC runs are performed and but only 10 of them are plotted to depict the system performance as shown in Figures 5a, 6a and 7a. MC results of the non-linear closed loop ADCS are compared to the linear covariance analysis results as shown in Figures 5b, 6b and 7b, which validates the usefulness and accuracy of linear covariance analysis.

The 3-axes estimation error determined by the linear covariance analysis matches the Monte Carlo

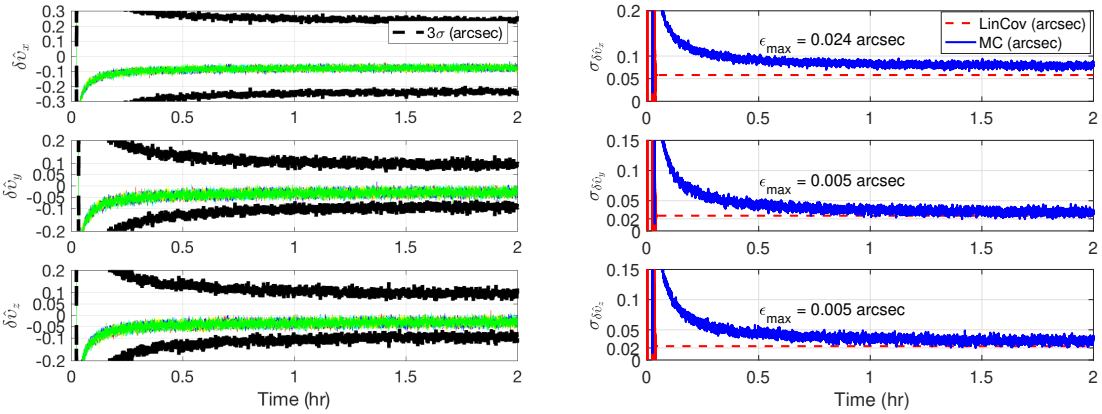

(a) Monte Carlo results for non-linear closed-loop ACDS with 3-σ statistics.

(b) Comparison of 1-σ Monte Carlo results to 1-σ linear covariance analysis.

Figure 5: Attitude estimation errors for 3-axes spacecraft.

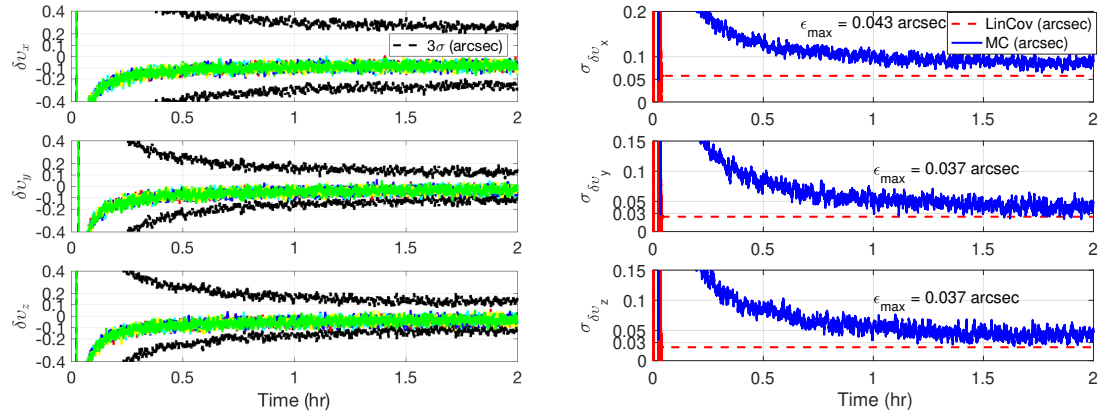

(a) Monte Carlo results for non-linear closed-loop ACDS with 3-σ statistics.

(b) Comparison of 1-σ Monte Carlo results to 1-σ linear covariance analysis.

Figure 6: True attitude dispersion for 3-axes spacecraft.

results with a maximum deviation of $\epsilon_{max} = 0.024$ arcsec in the x-axis and $\epsilon_{max} = 0.005$ arcsec in the y- and z-axes, where ϵ_{max} is the maximum difference between the Monte Carlo and linear covariance $1-\sigma$ data. The 3-axes true attitude dispersion from linear covariance analysis matches the Monte Carlo results with a maximum deviation of $\epsilon_{max} = 0.043$ arcsec in the x-axis and $\epsilon_{max} = 0.037$ arcsec in the y- and z-axes. Finally, the 3-axes control effort dispersion from linear covariance analysis matches the Monte Carlo results with a maximum deviation of $\epsilon_{max} = 5.5{\cdot}10^{-4}$ Nm in the x-axis and $\epsilon_{max} = 2.7 \cdot 10^{-4}$ Nm in the y- and z-axes.

CONCLUSION

In this paper linear covariance analysis of closed-loop ADCS of IRASSI's 3-axes spacecraft is performed that requires sub-arcsec pointing. Sources of errors in its closed-loop ADCS are the er-

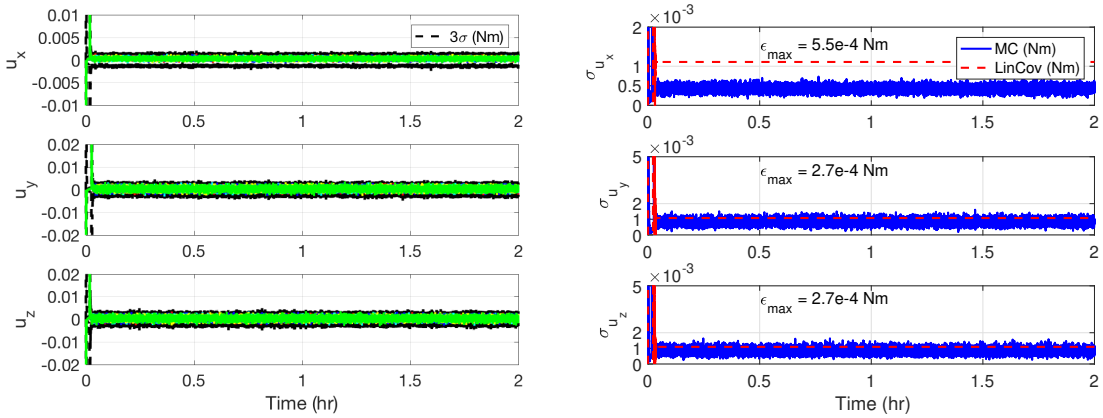

(a) Monte Carlo results for non-linear closed-loop ACDS with 3-σ statistics.

(b) Comparison of 1-σ Monte Carlo results to 1-σ linear covariance analysis.

Figure 7: Control effort dispersion for 3-axes spacecraft.

rors from the gyro, the external disturbance torques from the gravity-gradient, the solar radiation pressure and a random disturbance moment to account for other unforeseeable or unmodeled disturbances, control bias and wheel misalignments, a suboptimal MEKF with model replacement and a SMC that provides suboptimal tracking performance due to usage of saturation function. Covariance analysis equations are developed by creating a dimensionally large state vector comprising the navigation state vector and the true state vector which results in a large linear time-varying model of the entire closed-loop system. The variances of the true and expected attitude estimation errors, variances of true pointing errors of the closed-loop system and variance of the required control effort are validated using nonlinear Monte Carlo analysis. The implementation substantiates the claim that linear covariance analysis can be a useful tool for preliminary ADCS design. The usefulness, accuracy and efficiency of the linear covariance analysis for closed-loop ADCS is thus demonstrated. This error analysis also provides an indication of the contributions of various error sources to the uncertainties in the closed loop ADCS.

APPENDIX

$$\mathbf{A} = \begin{bmatrix} -[\boldsymbol{\omega}_N\times] & I_{3\times3} & 0_{3\times3} & 0_{3\times15} \\ 0_{3\times3} & A_\omega & \mathbf{J}_0^{-1} & 0_{3\times15} \\ 0_{18\times3} & 0_{18\times3} & 0_{18\times3} & 0_{18\times15} \end{bmatrix} \tag{78a}$$

$$\mathbf{A}_\omega = \mathbf{J}_0^{-1}([(\mathbf{J}_0\boldsymbol{\omega}_N)\times] - [\boldsymbol{\omega}_N\times]\,\mathbf{J}_0) \tag{78b}$$

$$\mathbf{G} = \begin{bmatrix} 0_{3\times3} \\ \mathbf{J}_0^{-1} \\ 0_{18\times3} \end{bmatrix}, \quad \mathbf{B} = \begin{bmatrix} 0_{3\times3} & 0_{3\times3} & 0_{3\times3} & 0_{3\times3} \\ 0_{3\times3} & 0_{3\times3} & \mathbf{J}_0^{-1} & \mathbf{J}_0^{-1} \\ 0_{6\times3} & 0_{6\times3} & 0_{6\times3} & 0_{6\times3} \\ 0_{3\times3} & I_{3\times3} & 0_{3\times3} & 0_{3\times3} \\ 0_{9\times3} & 0_{9\times3} & 0_{9\times3} & 0_{9\times3} \end{bmatrix} \tag{79}$$

$$\mathbf{H}_{gyro} = [0_{3\times3} \quad I_{3\times3} \quad 0_{3\times6} \quad I_{3\times3} \quad \mathbf{A}_{kU}(\boldsymbol{\omega}_N) \quad \mathbf{A}_{kL}(\boldsymbol{\omega}_N) \quad \mathbf{D}(\boldsymbol{\omega}_N)] \tag{80}$$

$$\mathbf{G}_x = \left[\frac{\mathbf{J}_0 \Lambda}{2} \operatorname{sign}(\delta q_4)[\boldsymbol{\omega}_N \times] \quad \mathbf{A}_\tau \quad -I_3 \quad 0_{3\times 15} \right], \quad \mathbf{G}_\zeta = [0_{3\times 6} \quad -I_3 \quad -I_3] \tag{81}$$

$$\mathbf{A}_\tau = [\boldsymbol{\omega}_N \times]\, \mathbf{J}_0 - [(\mathbf{J}_0 \boldsymbol{\omega}_N) \times] - \frac{\mathbf{J}_0 \Lambda}{2} \operatorname{sign}(\delta q_4) \tag{82}$$

$$\mathbf{H} = [I_3 \quad 0_{3\times 21}], \quad \mathbf{H}_f = [I_3 \quad 0_{3\times 3}] \tag{83}$$

$$\mathbf{A}_f = \begin{bmatrix} -[\boldsymbol{\omega}_N \times] & -I_{3\times 3} \\ 0_{3\times 3} & 0_{3\times 3} \end{bmatrix}, \quad \mathbf{G}_\omega = \begin{bmatrix} I_{3\times 3} \\ 0_{3\times 3} \end{bmatrix}, \quad \mathbf{B}_f = \begin{bmatrix} -I_{3\times 3} & 0_{3\times 3} \\ 0_{3\times 3} & I_{3\times 3} \end{bmatrix} \tag{84}$$

$$\mathbf{G}_{f_{\hat{x}}} = \left[\frac{\mathbf{J}_0 \Lambda}{2} \operatorname{sign}(\delta \hat{q}_{f_4})[\boldsymbol{\omega}_N \times] \quad -\mathbf{A}_{f_\tau} \right] \tag{85}$$

$$\mathbf{A}_{f_\tau} = [\boldsymbol{\omega}_N \times]\, \mathbf{J}_0 - [(\mathbf{J}_0 \boldsymbol{\omega}_N) \times] - \frac{\mathbf{J}_0 \Lambda}{2} \operatorname{sign}(\delta \hat{q}_{f_4}) \tag{86}$$

$$\mathbf{M}_x = [I_{N_x \times N_x} \quad 0_{N_x \times N_f}], \quad \mathbf{M}_f = [0_{N_f \times N_x} \quad I_{N_f \times N_f}] \tag{87}$$

$$\mathbf{G}_{\boldsymbol{\tau} gyro} = \mathbf{A}_{f_\tau} \mathbf{H}_{gyro}, \quad \mathbf{B}_\tau = \mathbf{A}_{f_\tau} [I_{3\times 3} \quad 0_{3\times 9}] \tag{88}$$

$$\mathbf{B}_{fX} = \mathbf{G}_\omega \begin{bmatrix} I_{3\times 3} & 0_{3\times 9} \end{bmatrix}, \quad \mathbf{A}_{fX} = \mathbf{G}_\omega \mathbf{H}_{gyro}, \quad \Delta\boldsymbol{\omega} = -[\boldsymbol{\omega}_N \times] \delta \mathbf{J} \boldsymbol{\omega}_N \tag{89}$$

$$\Delta\boldsymbol{\tau} = -\mathbf{J}_0 \boldsymbol{\varepsilon} sat(\boldsymbol{\sigma}_i, e_{bl_i}), \quad \Delta\boldsymbol{\tau}_f = -\mathbf{J}_0 \boldsymbol{\varepsilon} sat(\hat{\boldsymbol{\sigma}}_i, e_{bl_i}) \tag{90}$$

$$\Delta\mathbf{X} = \Delta\boldsymbol{\tau}_f + \Delta\boldsymbol{\omega} = -[\boldsymbol{\omega}_N \times] \delta \mathbf{J} \boldsymbol{\omega}_N - \mathbf{J}_0 \varepsilon sat(\hat{\boldsymbol{\sigma}}_i, e_{bl_i}) \tag{91}$$

$$\mathbf{M} = \begin{bmatrix} I_{3\times 3} & 0_{3\times 9} & 0_{3\times 3} & 0_{3\times 9} \\ 0_{3\times 3} & 0_{3\times 9} & I_{3\times 3} & 0_{3\times 9} \end{bmatrix} \tag{92}$$

$$\mathbf{P}_{disp_0} = blkdiag([\sigma^2_{\delta\upsilon} \;\; \sigma^2_{\delta\omega} \;\; \sigma^2_{b_{act}} \;\; \sigma^2_{\epsilon_{act}} \;\; \sigma^2_{b_\omega} \;\; \sigma^2_{k_U} \;\; \sigma^2_{k_L} \;\; \sigma^2_s]) \tag{93}$$

REFERENCES

[1] H. Linz, D. Bhatia, L. Buinhas, M. Lezius, E. Ferrer, and e. al., "InfraRed Astronomy Satellite Swarm Interferometry (IRASSI): Overview and study results," *Advances in Space Research*, Vol. 65, Jun 2020, 10.1016/j.asr.2019.06.022.

[2] D. Bhatia, "Attitude Determination and Control system design of sub-arcsec pointing IRASSI spacecraft," *Journal of Guidance, Control and Dynamics*, 2020. submitted.

[3] D. Bhatia, U. Bestmann, and P. Hecker, "High Accuracy Attitude Determination Estimator System for IRASSI interferometer Spacecraft," Vol. 17, 27th AAS/AIAA Space Flight Mechanics Meeting,February 5-9, 2017, San Antonio, Texas, USA, 2017.

[4] D. Bhatia, U. Bestmann, and P. Hecker, "High Accuracy Pointing Attitude Determination Estimator System for the future InfraRed Astronomy Satellite Swarm Interferometer," 10th International ESA Conference on Guidance, Navigation and Control Systems, 29 May-2 June, 2017, Salzburg, Austria, 2017.

[5] D. Bhatia and P. Hecker, "Disturbance-based High-Order Sliding Mode Observer-based Control for Spacecraft High Accuracy Pointing," Vol. 18, AAS/AIAA Astrodynamics Specialist Conference, August 19-23, 2018, Snowbird, Utah, USA, 2018.

[6] E. Brucker and P. Gurfil, "Analysis of gravity-gradient-perturbed rotational dynamics at the collinear Lagrange points," *The Journal of Astronautical Sciences*, Vol. 55, No. 3, 2007, pp. 271–291.

[7] O. Montenbruck and E. Gill, *Satellite orbits: models, methods and applications*. Berlin Heidelberg, Germany: Springer Science and Business Media, 2012. ISBN: 978-3-642-58351-3.

[8] F. L. Markley and J. L. Crassidis, *Fundamentals of Spacecraft Attitude Determination and Control*. New Jersey, USA: Space Technology Library, Springer, 2014. ISBN: 978-1-4939-0802-8.

[9] D. K. Geller, "Linear Covariance techniques for orbital rendezvous analysis and autonomous onboard mission planning," *Journal of Guidance, Control and Dynamics*, Vol. 29, No. 6, 2006.

[10] N. Leiter and D. K. Geller, *Linear Covariance techniques for Closed-Loop Attitude Determination and Control Analysis*. Berlin, Heidelberg: ENCS, Springer, 2012.

[11] R. H. Battin, *An Introduction to the Mathematics and Methods of Astrodynamics*. New York, USA: AIAA Education Series, 1987.